Proceedings of the ASME 2010 3rd Joint US-European Fluids Engineering Summer Meeting and 8th International Conference on Nanochannels, Microchannels, and Minichannels
FEDSM-ICNMM2010
August 1-5, 2010, Montreal, Canada

FEDSM-ICNMM2010-30103

EFFICIENT SIMULATION OF FULLY COUPLED WAVE-BODY INTERACTIONS USING A SHARP INTERFACE IMMERSED-BOUNDARY/LEVEL-SET METHOD

Jianming Yang *
IIHR – Hydroscience and Engineering
University of Iowa
Iowa City, IA 52242
Email: jianming-yang@uiowa.edu

Frederick Stern
IIHR – Hydroscience and Engineering
University of Iowa
Iowa City, IA 52242
Email: frederick-stern@uiowa.edu

ABSTRACT

In this paper, some recent progress toward the prediction of fully coupled wave-body interactions using a sharp interface immersed-boundary/level-set method is presented. A non-iterative strong coupling scheme for the fluid motion and rigid body dynamics is adopted by utilizing a non-inertial reference frame attached to the solid body. The combination of this scheme with the previous immersed-boundary/level-set method gives a robust and efficient tool for the prediction of solid body motions in waves. Several examples are presented to demonstrate the applicability of the new method. Possible further developments are discussed.

INTRODUCTION

Wave-body interactions are of interest in many engineering areas such as ocean, coastal, civil, and environmental engineering. The physics involved in wave-body interactions, e.g., multiphase turbulent flows of wind, current, and waves, dynamics of stationary/moving solid/deformable structures, and the interactions between the fluids and structures, is very complicated and presents significant challenges to theoretical, experimental, and computational studies of these phenomena.

Ship hydrodynamics is a typical field with a focus on wave-body interactions. The prediction of ship motions is the primary task of computational ship hydrodynamics, since ship motions are ubiquitous in all major areas of ship hydrodynamics, such as sinkage and trim in resistance and propulsion, pitch, heave, and roll in seakeeping, surge, sway, and yaw in maneuvering. Potential flow theory has been applied to ship motion prediction for a long time. However, the missing viscous effects and limited capacities for breaking waves in various potential flow solvers severely restrict their broader applications. RANS (Reynolds-averaged Navier-Stokes) solvers of various complexities have been developed in the last few decades for ship hydrodynamics problems beyond the reach of general potential solvers. CFDShip-Iowa version 4 is one of leading RANS codes for a wide range of ship hydrodynamics applications involving six DOF (degree-of-freedom) motions [1]. Unfortunately, these solvers usually require complicated three-dimensional (3D) mesh generation/deformation, block patching, or overset interpolation, which are absent in general potential flow solvers and practically excessive burdens on design engineers. The sharp interface immersed-boundary/level-set Cartesian grid method presented in [2], among other non-boundary-conforming methods, can essentially eliminate the complex grid generation process and be a promising approach for simple and efficient prediction of ship motions. In this method, the direct forcing immersed boundary formulation for moving boundary problems given in [3] was adopted; in addition, a level set method [4] was used for interface tracking with the ghost fluid method for the treatment of interface jump conditions [5]. Various cases of wave-body interactions with stationary or moving bodies from water entry and exit, to model scale ship flows were shown in [2] to demonstrate the accuracy and applicability of this method.

*Address all correspondence to this author.

The objective of the present study was to extend the sharp interface immersed-boundary/level-set method to fully coupled wave-body interactions. There are many different types of schemes available in the literature for fluid-structure interaction problems. It is well-known that the weak coupling schemes, usually, with a time lag of the forces/moments to the solid from the fluid phase, could become unstable in many circumstances; on the other hand, the strong coupling schemes are much stabler. In [6], a scheme of the latter category was developed to extend the direct forcing immersed boundary method in [3] to fluid-structure interaction problems involving multiple bodies. In this scheme, the fluid and the structure are treated as elements of a single dynamical system, and all the governing equations are integrated simultaneously and interactively in the time domain. As a predictor-corrector scheme, a few iterations between the fluid solver and the structure solver are involved. In each iteration, the positions of the immersed structures will be changed and the relationship between the grid and the immersed boundaries has to be redefined; moreover, the pressure Poisson equation has to be solved. Therefore, an efficient setup procedure for the immersed boundaries is of importance. And the cost of the Poisson solver is critical. In many applications, fast Poisson solvers utilizing FFT (fast Fourier transform) and cyclic reduction can be very useful to reduce the computational time. For example, the strong coupling scheme in [6] was used in [7] to simulation the pulsatile flow through an aortic bileaflet mechanical heart valve. However, for the two-phase flows in wave-body interactions, the fast Poisson solvers cannot be applied directly and usually iterative solvers are used. The cost of the pressure Poisson solver will be much higher in an iterative strong coupling scheme for wave-body interactions.

An alternative direct forcing immersed boundary approach for fluid-structure interactions given in [8] avoids the iterations in many strong coupling schemes by adopting a non-inertial reference frame. With such a frame fixed to the body, there is no relative motion between the body and the grid; the immersed boundary only needs to be set up once at the beginning of the simulation. More importantly, with an explicit, linear momentum forcing, a simple linear relationship between the fluid forces/moments acting on the body and the linear/angular velocities of the body was identified in [8], which enables a strongly coupled, direct update of the body velocities without iterations. In addition, the approach can effectively removes the wiggles in the forces/moments otherwise exist in many immersed boundary methods due to the motions of immersed boundaries on the underlying fixed grid. However, a major limitation of this method is that only the cases with a single rigid body can be handled. The use of non-inertial reference frame also introduces some complications in the treatment of domain boundary conditions, especially, at the inflow and outflow boundaries. Despite these limitations/complications, the method can still find its application in many circumstances.

A crucial aspect of the immersed boundary methods, especially, when dealing with fluid-structure interaction problems, is the evaluation of forces/moments from/to the immersed bodies. In many direct forcing approaches, the effects of the immersed bodies are fully represented by the extra forcing term added to the momentum equation. Therefore, for these approaches, a straightforward way of evaluating the forces/moments is to perform an integration of the forcing term pointwise. Actually, the method in [8] was built on top of this concept. On the other hand, in many other direct forcing approaches, an explicit momentum forcing term barely exists or is hard to define due to the extra manipulation of the governing equations or the solution itself. Usually, in these methods, the immersed boundaries have to be discretized into a triangulation (segments in 2D) with elements of size comparable with the local grid cells, then the shear stresses and pressure are calculated for each elements and the integration of forces/moments from all elements gives the final results. This approach was adopted in [3] and [6]. Due to many additional parameters such as size of surface triangle elements, distance away from the surface to interpolate velocity/pressure, this approach can be quite involved in algorithm and be sensitive to the choices of different parameters. In general, the evaluation of forces/moments is used as a post-processing step in the simulations of fluid-structure interactions. However, in [8], this step was combined into the fluid-structure coupling process in a non-inertial reference frame as discussed in the previous paragraph. And it was turned out that the iterations between the fluid and structure solvers, which are inevitable if the body has relative motions to the grid and/or the forces/moments are calculated with a complete solution, could be eliminated.

In this study, as a step forward for the prediction of six DOF ship motion on a Cartesian grid, the non-iterative strong coupling scheme in [8] was combined with the sharp interface immersed-boundary/level-set method in [2]. Due to the presence of the air-water interface, the whole gas-liquid-solid system considered here is more complicated than that in [8]. Therefore, the original formulation will be re-derived for a three-phase system with multiple material interfaces. Also, some preliminary simulation results of wave-body interaction problems will be presented.

MATHEMATICAL MODEL

In general, the mathematical model used in this study follows what presented in [2]. For completeness, the basic governing equations will be given here in addition to the definition of the non-inertial reference frame to be used and the dynamical equations for rigid body motions.

Non-Inertial Reference Frame

The conventional transformation of the Navier-Stokes equations from an inertial reference frame to a non-inertial reference

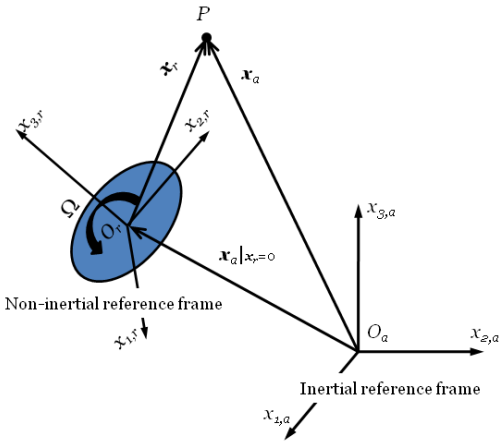

FIGURE 1. RELATIONSHIP BETWEEN THE INERTIAL AND NON-INERTIAL REFERENCE FRAMES.

frame will result in various source terms in the equations, such as the Euler, Coriolis and centrifugal forces. These terms are difficult to be formulated in conservative forms and the explicit treatment of these terms in a rotational system could be the source of numerical instability. In [9], a conservative formulation of the Navier-Stokes equations in a non-inertial reference frame was presented. Like [8], this formulation was also adopted here.

As shown in Fig. 1, a point P in space represented by $\mathbf{x}_a$ in the inertial reference frame will be converted to $\mathbf{x}_r$ in the non-inertial reference frame through the following equation:

$$\mathbf{x}_r = \mathbb{R}^T \left(\mathbf{x}_a - \mathbf{x}_a|_{\mathbf{x}_r=0} \right), \tag{1}$$

where the subscripts a and r represent the inertial and non-inertial reference frames, respectively, $\mathbb{R}^T$ is the transpose of the rotation matrix $\mathbb{R}$ between these two coordinate systems, and $\mathbf{x}_a|_{\mathbf{x}_r=0}$ is the position vector of the origin of non-inertial reference frame with respect to the inertial frame. The time derivative of Eq. (1) in the inertial frame can be derived as

$$\left(\frac{\partial \mathbf{x}_r}{\partial t} \right)_a = \mathbb{R}^T \frac{\mathrm{d}\mathbf{x}_a}{\mathrm{d}t} - \mathbb{R}^T \frac{\mathrm{d}\mathbf{x}_a|_{\mathbf{x}_r=0}}{\mathrm{d}t}, \tag{2}$$

with t the time, $()_a$ the time derivative in the inertial reference frame. It can be converted to the time derivative in the non-inertial reference frame represented by $()_r$ as

$$\left(\frac{\partial \mathbf{x}_r}{\partial t} \right)_a = \left(\frac{\partial \mathbf{x}_r}{\partial t} \right)_r + \Omega \times \mathbf{x}_r = \mathbf{u}_r + \mathbf{w} = \mathbb{R}^T \mathbf{u}_a - \mathbf{v} \tag{3}$$

with $\mathbf{u}_r = (\partial \mathbf{x}_r / \partial t)_r$ the relative velocity vector in the non-inertial reference frame, usually employed in the conventional transformation as the primitive variables, $\mathbf{v} = \mathbb{R}^T (\mathrm{d}\mathbf{x}_a|_{\mathbf{x}_r=0}/\mathrm{d}t)$ the translational velocity of the origin of the body-fixed coordinate in the non-inertial frame, Ω the angular velocity of the the body about the origin of the non-inertial frame, and $\mathbf{w} = \Omega \times \mathbf{x}_r$.

The salient feature of the conservative form by Beddhu et al. [9] is the use of the following velocity vector in the Navier-Stokes equations:

$$\mathbf{u} = \mathbf{u}_r + \mathbf{v} + \mathbf{w} = \mathbb{R}^T \mathbf{u}_a. \tag{4}$$

This formulation can ameliorate the difficulties of boundary conditions treatment when a non-inertial reference frame and the relative velocity vector $\mathbf{u}_r$ are used, as the above conversion is much simpler than that from $\mathbf{u}_a$ to $\mathbf{u}_r$.

The rotation matrix or the orientation of a rigid body can be represented by the Euler angles. However, a phenomenon called gimbal lock in which one degree of freedom of rotation is lost can be resulted from the Euler angle formulation. The quaternion representation, which has no gimbal lock problem, is adopted in the present study. For the rotation of an angle θ about an axis $\mathbf{n} = (n_1, n_2, n_3)$, the quaternion representation will be

$$\mathbf{q} = (\cos\frac{\theta}{2},\ n_1 \sin\frac{\theta}{2},\ n_2 \sin\frac{\theta}{2},\ n_3 \sin\frac{\theta}{2}) = (a,\ b,\ c,\ d), \tag{5}$$

And the rotation matrix $\mathbb{R}$ for such a rotation can be given as

$$\mathbb{R} = \begin{pmatrix} a^2+b^2-c^2-d^2 & 2bc-2ad & 2ac+2bd \\ 2ad+2bc & a^2-b^2+c^2-d^2 & 2cd-2ab \\ 2bd-2ac & 2ab+2cd & a^2-b^2-c^2+d^2 \end{pmatrix}. \tag{6}$$

The evolution of the quaternion is given by

$$\frac{\mathrm{d}\mathbf{q}}{\mathrm{d}t} = \frac{1}{2}\mathbf{q} \star (0, \Omega), \tag{7}$$

where the symbol $\star$ represents the quaternion multiplication operator and $(0, \Omega)$ represents a quaternion with a zero scalar part and the angular velocity vector as the vector part.

Navier–Stokes Equations

In the non-inertial reference frame defined above, the Navier–Stokes equations governing the incompressible viscous flows of two immiscible fluids, e.g., air and water, can be written as:

$$\left(\frac{\partial \mathbf{u}}{\partial t} \right)_r + \nabla \cdot [(\mathbf{u} - \mathbf{v} - \mathbf{w})\,\mathbf{u} + \mathbf{u}\mathbf{w}] = \frac{1}{\rho} \nabla \cdot (-p\mathbf{I} + \mathbf{T}) + \mathbf{g} + \mathbf{f}, \tag{8}$$

$$\nabla \cdot \mathbf{u} = 0, \tag{9}$$

where p is the pressure, $\mathbf{I}$ is the unit tensor, ρ is the density, $\mathbf{g}$ represents the gravity, $\mathbf{f}$ represents the momentum forcing term due to the immersed body, and $\mathbf{T}$ is the viscous stress tensor defined as

$$\mathbf{T} = 2\mu\mathbf{S}, \tag{10}$$

with μ the dynamic viscosity, $\mathbf{S}$ the strain rate tensor given by

$$\mathbf{S} = \frac{1}{2}\left[\nabla\mathbf{u} + (\nabla\mathbf{u})^T\right]. \tag{11}$$

There is an interesting link between this formulation and the formulation in an inertial reference frame with a moving grid and a colocated variable arrangement, which is commonly used in many finite volume, especially, commercial solvers. In the current method, since a staggered Cartesian grid is used, a contravariant vector basis has to be adopted. However, with a colocated grid, the vector basis in the body-fixed grid/coordinate can remain the same as the absolute (inertial) reference frame. Therefore, the rotation matrix defined above reduces to an identity matrix and the angular velocity vector due to the coordinate transformation becomes zero. And Eq. (8) becomes the governing equation for a moving grid system in an inertial reference frame. Of course, the definition of grid velocity vector $\mathbf{v}$ can be generalized to deformable grids.

Interface Modeling

Interface Tracking. The level set evolution equation [4] in the non-inertial reference frame can be used to track the position of the interface

$$\frac{\partial\phi}{\partial t} + (\mathbf{u} - \mathbf{v} - \mathbf{w})\cdot\nabla\phi = 0, \tag{12}$$

with the interface Γ given by the zero level set of the level set function, ϕ. The reinitialization equation [10] for the level set function is iteratively solved to keep ϕ as a signed distance function in the course of its evolution. Its form does not change under the coordinate transformation:

$$\frac{\partial\phi}{\partial\tau} + S(\phi_o)\left(|\nabla\phi| - 1\right) = 0, \tag{13}$$

where τ is the pseudo time for the iteration and $S(\phi_o)$ is the numerically smeared-out sign function, for details see [10].

Physical Properties. Each phase of constant density and viscosity can be easily defined by the level set function in the computational domain and sharp jumps of the fluid properties occur at the phase interface:

$$\begin{aligned}\rho &= \rho_G + (\rho_L - \rho_G)H(\phi),\\ \mu &= \mu_G + (\mu_L - \mu_G)H(\phi),\end{aligned} \tag{14}$$

where the subscripts G and L represent gas and liquid phase, respectively. The stepwise Heaviside function is defined as

$$H(\phi) = \begin{cases} 1, & \text{if} \quad \phi \geq 0 \\ 0, & \text{if} \quad \phi < 0 \end{cases}. \tag{15}$$

Jump Conditions. Since the flows considered here are viscous and no phase change occurred, the velocity across the interface Γ is continuous:

$$[\mathbf{u}] = 0, \tag{16}$$

where $[\,\cdot\,]$ indicates the jump at the interface, i.e., $f_L^I - f_G^I$ for a variable f with superscript I denotes interface.

The exact jump condition for stress is

$$\left[\mathbf{n}\cdot\left(-p\mathbf{I} + \mu\left(\nabla\mathbf{u} + (\nabla\mathbf{u})^T\right)\right)\cdot\mathbf{n}\right] = \sigma\kappa, \tag{17}$$

where σ is the coefficient of surface tension.

In this study, the surface tension and shear stress jump due to the viscosity jump $[\mu]$ at the interface was ignored and the above condition reduces to

$$[p] = 0. \tag{18}$$

Rigid Body Dynamics

The dynamics of a rigid body in a fluid-structure coupled system is described by

$$\mathbb{M}_\mathrm{s}\left(\frac{\mathrm{d}\mathbf{v}}{\mathrm{d}t}\right)_r + \mathbb{M}_\mathrm{s}\Omega\times\mathbf{v} = \mathbf{F}_\mathrm{N} + \mathbf{F}_\mathrm{e}, \tag{19}$$

$$\mathbb{I}_\mathrm{s}\left(\frac{\mathrm{d}\Omega}{\mathrm{d}t}\right)_r + \Omega\times(\mathbb{I}_\mathrm{s}\Omega) = \mathbf{T}_\mathrm{N} + \mathbf{T}_\mathrm{e}, \tag{20}$$

where $\mathbb{M}_\mathrm{s}$ is the mass of the solid body times a 3×3 identity matrix (tensor), $\mathbb{I}_\mathrm{s}$ is the moment of inertia of the body, $\mathbf{F}_\mathrm{N}$ and $\mathbf{T}_\mathrm{N}$ are the fluid forces and moments in the non-inertial reference frame, respectively, and, following Kim and Choi [8], all other sources of forces and moments are represented by $\mathbf{F}_\mathrm{e}$ and $\mathbf{T}_\mathrm{e}$,

respectively. The forces and moments $\mathbf{F}_\mathrm{N}$ and $\mathbf{T}_\mathrm{N}$ can be transformed to those in the inertial reference frame as

$$\mathbf{F}_\mathrm{I} = \mathbb{R}\mathbf{F}_\mathrm{N}, \tag{21}$$

$$\mathbf{T}_\mathrm{I} = \mathbb{R}\mathbf{T}_\mathrm{N}, \tag{22}$$

respectively.

NUMERICAL METHOD

The details of many aspects of the numerical method used in this work have been presented in several previous studies [3,6,2]. Here only a summary of each module and the differences from the previous work, especially, the non-iterative fluid-structure coupling algorithm, will be focused on.

Navier-Stokes Solver

A fractional-step method is employed for velocity-pressure coupling, in which a pressure Poisson equation is solved to enforce the continuity equation. A second-order Adams–Bashforth scheme is used for time advancement. The algorithm can be written as follows:

$$\frac{\hat{u}_i - u_i^{n-1}}{\Delta t} = \mathrm{RHS}_i^n + f_i^n \tag{23}$$

$$= \frac{3}{2}H_i(\mathbf{u}^{n-1}) - \frac{1}{2}H_i(\mathbf{u}^{n-2}) - \frac{1}{\rho^n}\frac{\partial p^{n-1}}{\partial x_i} + g_i^n + f_i^n,$$

$$\frac{\partial}{\partial x_i}\left(\frac{1}{\rho}\frac{\partial \psi}{\partial x_i}\right) = \frac{1}{\Delta t}\frac{\partial \hat{u}_i}{\partial x_i}, \tag{24}$$

$$u_i^n = \hat{u}_i - \Delta t \frac{1}{\rho^n}\frac{\partial \psi}{\partial x_i}, \tag{25}$$

$$p^n = p^{n-1} + \psi, \tag{26}$$

where superscript n denotes time step, subscript $i = 1,2,3$ represents i-coordinate in the non-inertial reference frame, $\hat{u}$ is the intermediate velocity, H is a spatial operator containing the convective and viscous terms, and ψ is the pressure increment.

The spatial derivatives are discretized using second-order central difference schemes, except for the convective terms, a third-order QUICK (Quadratic Upwind Interpolation for Convective Kinematics) scheme [11] and higher-order WENO schemes [12] are also available. The Poisson equation is solved using a semi-coarsening multigrid solver from the Hypre package developed at Lawrence Livermore National Laboratory [13]. In general, this is the most expensive part of the whole algorithm and uses more than 90 percent of the CPU time in each time step.

Level Set Solver

At each time step, the air-water interface is advected first by using the level set method. The local (narrow band) level set method by Peng et al. [14] is adopted to solve the level set evolution and reinitialization equations using a fifth-order HJ WENO scheme [15] for the spatial discretization and a third-order TVD Runge–Kutta scheme [16] for time advancement. With an updated interface, the fluid properties, i.e., density and viscosity, are defined accordingly.

Immersed Boundary Treatment

In a direct forcing immersed boundary method, usually the effect of an immersed rigid body on the fluid flow is represented by a momentum forcing term in the momentum equation. However, the evaluation of this forcing term can be substantially different in different approaches. A simple and straightforward approach is to modify/reconstruct the solution near the immersed boundary such as the boundary conditions on the immersed boundary are satisfied. Usually, the modification/reconstruction is performed with an explicitly predicted solution to further simplify the process, although with a splitting error due to the use of predicted instead of the real solution. For example, with the solutions from the previous time steps available, the predicted solution for time step t^n will be

$$\hat{\mathbf{u}} = \mathbf{u}^{n-1} + \Delta t \mathbf{RHS}^n. \tag{27}$$

Note the forcing term is not included in the above equation. In order to satisfy the the velocity distribution inside and near the immersed boundary, a correction has to be applied to the predicted velocity field in a form of $\mathbf{u}^n_{forcing} = \hat{\mathbf{u}} + \Delta t \mathbf{f}^n$, or,

$$\mathbf{f}^n = \frac{\mathbf{u}^n_{forcing} - \mathbf{u}^{n-1}}{\Delta t} - \mathbf{RHS}^n, \tag{28}$$

where $\mathbf{u}^n_{forcing}$ includes the effect of the immersed body. Inside the solid, rigid body motion is imposed and

$$\mathbf{u}^n_{forcing} = \mathbf{u}^n_{solid} = \mathbf{v}^n + \Omega^n \times \mathbf{x}_r. \tag{29}$$

Unfortunately, at the forcing points, which are points in the fluid phase but with neighboring point in the solid phase, a local reconstruction is necessary to obtain $\mathbf{u}^n_{forcing}$. In [3] and [6], a linear interpolation stencil utilizing the velocity components or any other variables from the immersed boundary and the surrounding fluid points was written as

$$\varphi = a + b\,x + c\,y + d\,z, \tag{30}$$

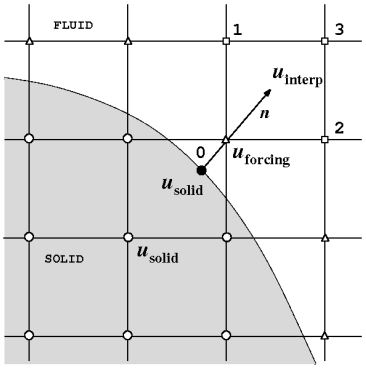

FIGURE 2. IMMERSED BOUNDARY TREATMENT.

and a 4×4 matrix was formed by representing all stencil points with it. Then this matrix was inverted to give the coefficients and the interpolation at a forcing point was evaluated with ease. To facilitate the fluid-structure coupling algorithm in [8], the formulation is changed slightly as shown in Fig. 2. At a forcing point, the velocity component is interpolated using

$$\mathbf{u}^n_{forcing} = \lambda \mathbf{u}^n_{solid} + (1-\lambda)\mathbf{u}_{interp}, \tag{31}$$

with $\mathbf{u}_{interp}$ again interpolated from the surrounding fluid points such as points 1, 2, and/or 3 in Fig. 2. λ is a linear weighting factor determined by the locations of $\mathbf{u}^n_{forcing}$, $\mathbf{u}^n_{solid}$, and $\mathbf{u}_{interp}$. Note that $\mathbf{u}^n_{solid}$ is unknown in a fluid-structure interaction problem and has to be obtained by solving the dynamic equations for rigid body motion.

Forces and Moments

As discussed above, the forcing term $\mathbf{f}^n$ added to the momentum equation represents the effects of the immersed body on the fluid flow, plus, the forces required to impose a rigid body motion of the portion of fluid enclosed by the immersed boundary. On the other hand, the total forces and moments applied to the solid body by the fluid can be derived from $\mathbf{f}^n$ as follows

$$\mathbf{F}^n_N = -\left[\int_V \rho \mathbf{f}^n dV - \mathbb{M}_f\left(\frac{\mathbf{v}^n-\mathbf{v}^{n-1}}{\Delta t} + \Omega^{n-1}\times\mathbf{v}^{n-1}\right)\right], \tag{32}$$

$$\mathbf{T}^n_N = -\left[\int_V \rho \mathbf{x}_r\times\mathbf{f}^n dV - \left(\mathbb{I}_f\frac{\Omega^n-\Omega^{n-1}}{\Delta t} + \Omega^{n-1}\times\mathbb{I}_f\Omega^{n-1}\right)\right] \tag{33}$$

where $\mathbb{M}_f$ and $\mathbb{I}_f$ are the counterparts of $\mathbb{M}_s$ and $\mathbb{I}_s$, i.e., the mass and moment of inertia of the portion of fluid enclosed in the volume V defined by the immersed boundary.

In a gas-liquid-solid system, the contact line boundary condition has to be specified, e.g., as discussed in [2], at the triple point where the air-water interface intercepts the immersed boundary. In this procedure, the air-water interface is extended into the solid phase and changes its position in the course of simulation. With both air and water phases inside the solid, $\mathbb{M}_f$ and $\mathbb{I}_f$ will become functions of time and extra errors will be introduced into the evaluation of the forces and moments for enforcing the rigid body motion. To simplify the problem, in this study the volume enclosed by the immersed boundary was chosen to have a density of the heavier fluid phase, i.e., water. Fig. 3 illustrates this procedure. On the other hand, direct use of the solid density, if available, is also possible, but the condition number of the Poisson equation will be increased for the case of a rigid body that is much heavier/lighter than both fluid phases.

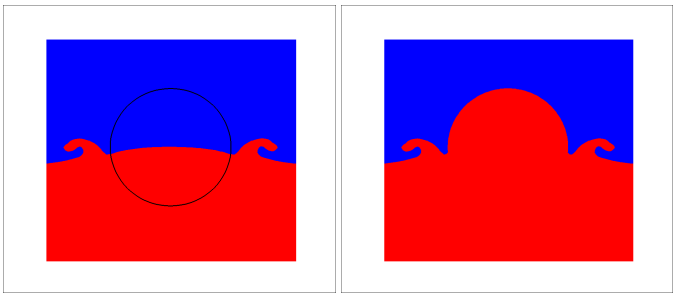

FIGURE 3. TREATMENTS OF CONTACT LINE BOUNDARY CONDITION AND INTERIOR OF THE SOLID BODY. LEFT: GAS-LIQUID INTERFACE ACROSS THE BODY; RIGHT: DENSITY PROFILE SHOWING SOLID FILLED WITH LIQUID.

From Eqs. (28) and (31), there is a clear dependence of $\mathbf{f}^n$ on the linear and angular velocities of the rigid body, which can be written as $\mathbf{X}^n = (\mathbf{v}^n, \Omega^n)^T$ for convenience. However, for a strong coupling scheme, the forces and moments at time step t^n, i.e., Eqs. (32) and (33), are required to solve the dynamic equation for rigid body motion to obtain $\mathbf{X}^n$. A particular advantage from the non-inertial reference frame, or, a body-fixed grid, is the prediction of position/orientation of the rigid body at time t^n becomes unnecessary. More importantly, as shown by Kim and Choi [8], if a provisional step of using $\mathbf{X}^{n-1}$ to evaluate the forcing term is taken, and the resulting forcing term is written as $\mathbf{f}^*$, then from Eqs. (28) and (31), the following relationship between the difference of these two forcing terms and the body velocity vector increment $\Delta\mathbf{X} = \mathbf{X}^n - \mathbf{X}^{n-1}$ exists:

$$\begin{aligned}\mathbf{f}^n - \mathbf{f}^* &= \frac{\mathbf{u}^n_{forcing} - \mathbf{u}^*_{forcing}}{\Delta t} \\ &= \lambda\frac{\mathbf{u}^n_{solid} - \mathbf{u}^{n-1}_{solid}}{\Delta t} \\ &= \frac{\lambda}{\Delta t}\left[\left(\mathbf{v}^n - \mathbf{v}^{n-1}\right) + \mathbf{x}_r\times\left(\Omega^n - \Omega^{n-1}\right)\right],\end{aligned} \tag{34}$$

noting that in Eq. (31), $\mathbf{u}_{interp}$ is obtained from an interpolation of the intermediate velocity field $\hat{\mathbf{u}}$ and no information of body velocity is required. Therefore, similar to [8], Eqs. (32) and (33)

can be written as

$$\begin{aligned}\mathbf{F}_N^n = &-\int_V \rho\left(\mathbf{f}^n-\mathbf{f}^*\right)\mathrm{d}V-\int_V \rho\mathbf{f}^*\mathrm{d}V\\ &+\mathbb{M}_\mathrm{f}\left(\mathbf{v}^n-\mathbf{v}^{n-1}\right)+\mathbb{M}_\mathrm{f}\left(\Omega^{n-1}\times\mathbf{v}^{k-1}\right),\end{aligned} \tag{35}$$

$$\begin{aligned}\mathbf{T}_N^n = &-\int_V \rho\mathbf{x}_r\times\left(\mathbf{f}^n-\mathbf{f}^*\right)\mathrm{d}V-\int_V \rho\mathbf{x}_r\times\mathbf{f}^*\mathrm{d}V\\ &+\mathbb{I}_\mathrm{f}\left(\Omega^n-\Omega^{n-1}\right)+\left(\Omega^{n-1}\times\mathbb{I}_\mathrm{f}\Omega^{k-1}\right),\end{aligned} \tag{36}$$

respectively. And the first terms in the right hand sides of these two equations become the following forms utilizing Eq. (34)

$$\int_V \rho\left(\mathbf{f}^n-\mathbf{f}^*\right)\mathrm{d}V=\frac{1}{\Delta t}\mathbb{A}_{3\times6}\left(\mathbf{X}^n-\mathbf{X}^{n-1}\right) \tag{37}$$

$$\int_V \rho\mathbf{x}_r\times\left(\mathbf{f}^n-\mathbf{f}^*\right)\mathrm{d}V=\frac{1}{\Delta t}\mathbb{B}_{3\times6}\left(\mathbf{X}^n-\mathbf{X}^{n-1}\right) \tag{38}$$

where $\mathbb{A}_{3\times6}$ and $\mathbb{B}_{3\times6}$ are determined by the interpolation factor λ, grid distribution $\mathbf{x}_r$, and density ρ. Unlike the case in [8], they have to be re-evaluated each time step due to the changes in ρ at the forcing points. Now the forces and moments can be combined as

$$\begin{aligned}\begin{bmatrix}\mathbf{F}_N^n\\ \mathbf{T}_N^n\end{bmatrix}=&\frac{1}{\Delta t}\left(\mathbb{K}-\mathbb{E}\right)\left(\mathbf{X}^n-\mathbf{X}^{n-1}\right)\\ &-\begin{bmatrix}\int_V \rho\mathbf{f}^*\mathrm{d}V\\ \int_V \rho\mathbf{x}_r\times\mathbf{f}^*\mathrm{d}V\end{bmatrix}+\begin{bmatrix}\mathbb{M}_\mathrm{f}\left(\Omega^{n-1}\times\mathbf{v}^{n-1}\right)\\ \Omega^{n-1}\times\left(\mathbb{I}_\mathrm{f}\Omega^{n-1}\right)\end{bmatrix},\end{aligned} \tag{39}$$

where

$$\mathbb{K}=\begin{bmatrix}\mathbb{M}_\mathrm{f} & \mathbf{0}\\ \mathbf{0} & \mathbb{I}_\mathrm{f}\end{bmatrix},\quad\text{and}\quad\mathbb{E}=\begin{bmatrix}\mathbb{A}_{3\times6}\\ \mathbb{B}_{3\times6}\end{bmatrix}. \tag{40}$$

Rigid Body Dynamics Solver

Similar to [8], a second-order, implicit, Crank-Nicolson scheme was used for the forces/moments in the discretized equations for rigid body dynamics, whereas all other terms were approximated using a second-order, explicit, Adams-Bashforth scheme. Eqs. (19) and (20) can be discretized as

$$\begin{aligned}\mathbb{M}_\mathrm{s}\frac{\mathbf{v}^n-\mathbf{v}^{n-1}}{\Delta t}=&\frac{1}{2}\left(\mathbf{F}_N^n+\mathbf{F}_N^{n-1}\right)+\frac{1}{2}\left(3\mathbf{F}_e^{n-1}-\mathbf{F}_e^{n-2}\right)\\ &-\frac{1}{2}\left(3\mathbb{M}_\mathrm{s}\Omega^{n-1}\times\mathbf{v}^{n-1}-\mathbb{M}_\mathrm{s}\Omega^{n-2}\times\mathbf{v}^{n-2}\right),\end{aligned} \tag{41}$$

$$\begin{aligned}\mathbb{I}_\mathrm{s}\frac{\Omega^n-\Omega^{n-1}}{\Delta t}=&\frac{1}{2}\left(\mathbf{T}_N^n+\mathbf{T}_N^{n-1}\right)+\frac{1}{2}\left(3\mathbf{T}_e^{n-1}-\mathbf{T}_e^{n-2}\right)\\ &-\frac{1}{2}\left(3\Omega^{n-1}\times\mathbb{I}_\mathrm{s}\Omega^{n-1}-\Omega^{n-2}\times\mathbb{I}_\mathrm{s}\Omega^{n-2}\right).\end{aligned} \tag{42}$$

Again, they can be combined and rewritten as

$$\begin{aligned}\mathbb{J}\left(\mathbf{X}^n-\mathbf{X}^{n-1}\right)=&\frac{1}{2}\left(\mathbb{K}-\mathbb{E}\right)\left(\mathbf{X}^n-\mathbf{X}^{n-1}\right)\\ &+\frac{\Delta t}{2}\mathbf{P}+\frac{3\Delta t}{2}\mathbf{Q}^{n-1}-\frac{\Delta t}{2}\mathbf{Q}^{n-2},\end{aligned} \tag{43}$$

where

$$\mathbb{J}=\begin{bmatrix}\mathbb{M}_\mathrm{s} & \mathbf{0}\\ \mathbf{0} & \mathbb{I}_\mathrm{s}\end{bmatrix},\quad\mathbf{Q}=\begin{bmatrix}\mathbf{F}_e\\ \mathbf{T}_e\end{bmatrix}-\begin{bmatrix}\mathbb{M}_\mathrm{s}\mathbf{w}\times\mathbf{v}\\ \mathbf{w}\times\left(\mathbb{I}_\mathrm{s}\mathbf{w}\right)\end{bmatrix} \tag{44}$$

and,

$$\mathbf{P}=-\begin{bmatrix}\int_V \rho\mathbf{f}^*\mathrm{d}V\\ \int_V \rho\mathbf{x}_r\times\mathbf{f}^*\mathrm{d}V\end{bmatrix}+\begin{bmatrix}\mathbb{M}_\mathrm{f}\left(\mathbf{w}^{k-1}\times\mathbf{v}^{k-1}\right)\\ \mathbf{w}^{k-1}\times\left(\mathbb{I}_\mathrm{f}\mathbf{w}^{k-1}\right)\end{bmatrix}+\begin{bmatrix}\mathbf{F}_N^{n-1}\\ \mathbf{T}_N^{n-1}\end{bmatrix}. \tag{45}$$

From Eq. (43), the velocity vector of the rigid body can be obtained from the following equation directly

$$\begin{aligned}\mathbf{X}^n=&\begin{pmatrix}\mathbf{v}^n\\ \Omega^n\end{pmatrix}=\mathbf{X}^{n-1}\\ &+\left[\mathbb{J}-\frac{1}{2}\left(\mathbb{K}-\mathbb{E}\right)\right]^{-1}\left[\frac{\Delta t}{2}\mathbf{P}+\frac{3\Delta t}{2}\mathbf{Q}^{n-1}-\frac{\Delta t}{2}\mathbf{Q}^{n-2}\right].\end{aligned} \tag{46}$$

With this updated velocity vector, the momentum forcing term $\mathbf{f}^n$ can be calculated and the the fluid flow solver can proceed to obtain the solution field at time t^n.

RESULTS

In this part, a case with prescribed motion is presented first to established the accuracy of the forces calculation, then several cases of fluid-structure interaction problems with predicted motions are demonstrated.

In-Line Oscillation of a Circular Cylinder

For an in-line oscillating circular cylinder in a fluid at rest, two key parameters are the Reynolds number, $Re=U_\mathrm{max}D/\nu$, and the Keulegan-Carpenter number, $KC=U_\mathrm{max}/fD$, where U_max is the maximum velocity of the cylinder, D is the diameter of the cylinder, ν is the kinematic viscosity of the fluid, and f is the characteristic frequency of the oscillation. The parameters from the experiments and numerical simulations in [17] were used here, i.e., $Re=100$ and $KC=5$. The prescribed translational motion of the cylinder is $x(t)=-A\sin(2\pi ft)$, where A is the amplitude of the oscillation. The size of computational domain is $50D\times30D$ in x and z, respectively, with the cylinder located at the center. A grid of 240×120 Near the cylinder the grid is approximately uniform in both directions with local spacing of $0.05D$.

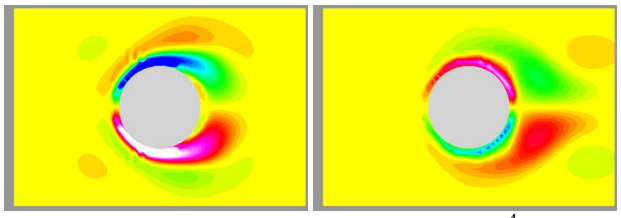

(a) $t = 0T$ (b) $t = \frac{4}{15}T$

(c) $t = \frac{8}{15}T$ (d) $t = \frac{12}{15}T$

FIGURE 4. VORTICITY CONTOURS AT FOUR DIFFERENT PHASE-ANGLES FOR AN IN-LINE OSCILLATING CYLINDER IN A FLUID AT REST AT $RE = 100$ AND $KC = 5$.

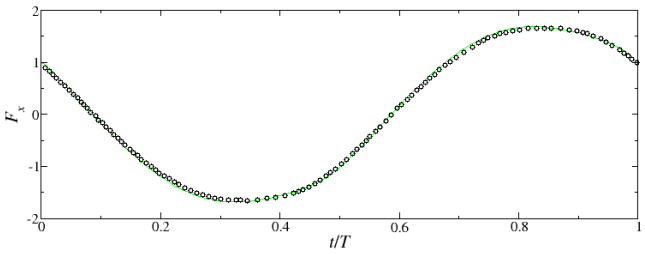

FIGURE 5. TIME HISTORY OF THE IN-LINE FORCE ACTING ON A CYLINDER OSCILLATING IN A FLUID AT REST AT $RE = 100$ AND $KC = 5$.

The computation was performed until periodic vortex shedding was established. In Fig. 4 the vorticity contours at four different phase-angles are shown. The results are in very good agreement with the corresponding results reported in [17].

In Fig. 5 the time history of the in-line force, $F_x(t)$, acting on the cylinder is shown in comparison with the reference simulation results. The agreement with the reference computations is very good. In [3], the force history of the same case is not as smooth as the present one. In an inertial reference frame, due to the relative motions between the cylinder and the grid, the interpolation stencil for a forcing point will be changed accordingly. Depending on the CFL numbers, within a few time steps, the fluid points involved in a stencil usually will be the same and only the coefficients in the stencil will be modified. If this is the case for most of the forcing points, a wiggle will not appear in the force evolution. Unfortunately, this is practically impossible

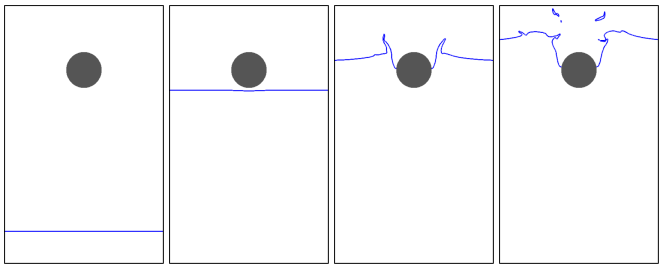

(a) $t = 0s$ (b) $t = 0.3s$ (a) $t = 0.35s$ (b) $t = 0.4s$

FIGURE 6. FREE SURFACE PROFILES AT SEVERAL INSTANCES DURING THE WATER IMPACT AND ENTRY OF A HALF BUOYANT CIRCULAR CYLINDER.

for a moving boundary problem in an inertial reference frame. However, with a non-inertial reference frame, all interpolation stencils keep the same in the course of body motion and a much smoother curve for force history can be obtained.

Water Impact of a Circular Cylinder

The impact and entry of a half-buoyant circular cylinder into an initially calm water surface is a fluid-structure interaction problem. Greenhow and Lin [18] studied this problem experimentally and the conditions were used in this work. A cylinder of diameter $D = 11$cm was dropped at a height of 0.5m from the free surface at time $t = 0$s. The impact on the free surface was occurred at about $t = 0.3$s. In this study, a grid of 120×500 was used to cover the computational domain. Around the cylinder and in the path of cylinder, or, the air-water interface in a non-inertial reference frame, a uniform grid spacing of $0.02D$ was used. The Reynolds number based on maximum velocity of the cylinder is around $Re = 2.9 \times 10^5$.

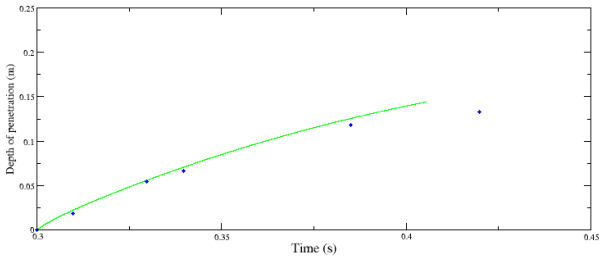

FIGURE 7. DEPTH OF PENETRATION OF A HALF BUOYANT CIRCULAR CYLINDER DURING THE WATER ENTRY PROCESS. LINE: SIMULATION; DOTS: EXPERIMENT [18].

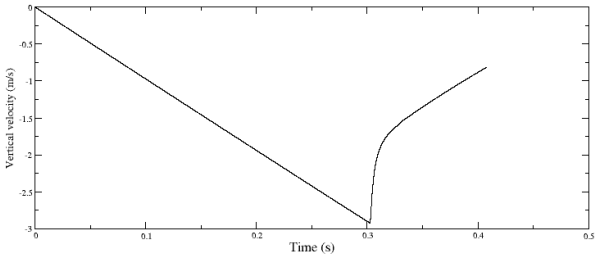

FIGURE 8. TIME HISTORY OF THE VERTICAL VELOCITY OF A HALF BUOYANT CIRCULAR CYLINDER DURING THE WATER IMPACT AND ENTRY PROCESS.

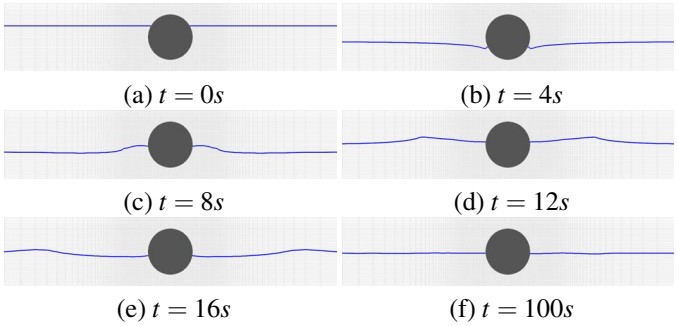

FIGURE 9. FREE SURFACE PROFILES DURING THE COURSE OF A HALF BUOYANT CIRCULAR CYLINDER REACHING ITS EQUILIBRIUM STATE.

Figure 6 shows the free surface profiles at several instances during the water impact and entry. After the cylinder penetrates the interface, two water jets are generated by the impact and the upper surface of the cylinder remains dry even after the top point of the cylinder is below the free surface.

The depth of penetration of the cylinder during the water entry process is shown and compared with the experimental data [18] in Fig. 7. The simulation results agree with the experimental data well, especially, during the initial stage. Fig. 8 shows the vertical velocity of the cylinder in the whole process. The velocity during the drop in the air has a slope of the gravitational acceleration. After the impact, the velocity exhibits a rapid decrease followed by a slow and steady one.

Equilibrium State of a Floating Circular Cylinder

In this case, a half-buoyant circular cylinder of diameter $D =$ 2m was held still with the center 0.5m below the free surface. It was released at time $t = 0$s. According to Archimedes' law, the cylinder reached its equilibrium state, in which half of the cylinder was above the free surface, after some time. The buoyancy force at the final equilibrium state should be $\frac{1}{8}\pi D^2 L\,\rho_{water} g$, which is 15.4kN for a cylinder of length $L = 1$m. This case was used in [19].

A grid of 200×120 was used in this simulation with a local grid spacing of $0.02D$ around the cylinder. Since a non-reflecting boundary condition was not applied in this study, the simulation took a long time to reach the equilibrium state. Fig. 9 shows the free surface profiles at several instances, e.g., the initial state of $3/4$ portion submerged and the final state of $1/2$ portion submerged. Fig. 10 shows the time history of the vertical force on the cylinder, after a long time, the equilibrium force 15.4kN is reached. The corresponding time history of the vertical velocity of the cylinder is shown in Fig. 11 and the approaching to a zero velocity is illustrated.

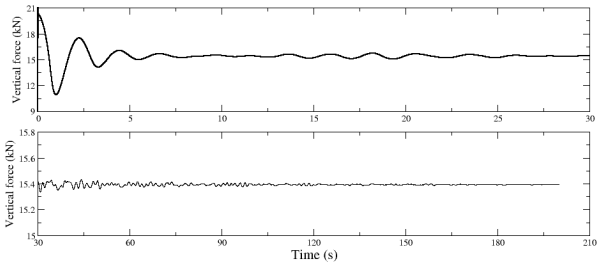

FIGURE 10. TIME HISTORY OF THE VERTICAL FORCE ON A HALF BUOYANT CYLINDER REACHING ITS EQUILIBRIUM STATE.

CONCLUSIONS AND FUTURE WORK

In this work, the sharp interface immersed-boundary/level-set method developed in [2] has been extended to fully coupled wave-body interaction problems. The non-iterative strong coupling scheme in [8] for an immersed boundary method in a non-inertial reference frame has been adopted for efficiency. The combination of this scheme with our method has been discussed in detail to highlight the differences of the treatment in a gas-liquid-solid system. Several cases have been tested to validate the computational method and demonstrate the applicability of the new method.

The cases with rotations were not considered in this work. Usually, in a inertial reference frame, the air-water interface can be aligned well with grid lines in one (e.g., the horizontal) direction. Then the grid in this direction can be locally refined to resolve the interface, whereas the other direction(s) can be stretched to save computational cost. However, in a non-inertial reference frame, such a stretched grid will not have enough resolution for the interface away from the solid body. To solve this problem, either an adaptive mesh refinement approach for the

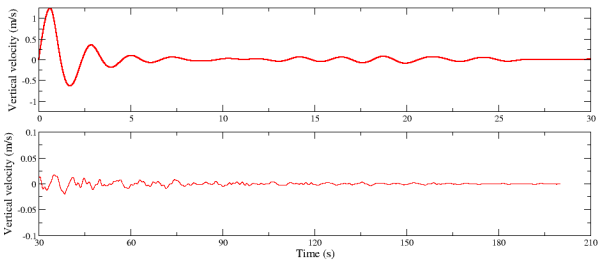

FIGURE 11. TIME HISTORY OF THE VERTICAL VELOCITY OF A HALF BUOYANT CYLINDER REACHING ITS EQUILIBRIUM STATE.

whole solver, or the refined level set grid method [20], in which only the level set equation is solved on a fine uniform Cartesian grid in a narrow band around the interface, can be used.

ACKNOWLEDGMENT

This work was sponsored by the Office of Naval Research (ONR) under grants N00014-01-1-0073 and N00014-06-1-0420, with Dr. Patrick Purtell as the program manager.

REFERENCES

[1] Carrica, P. M., Wilson, R. V., Noack, R. W., and Stern, F., 2007. "Ship motions using single-phase level set with dynamic overset grids". *Computers & Fluids,* ***36***(9), pp. 1415–1433.

[2] Yang, J., and Stern, F., 2009. "Sharp interface immersed-boundary/level-set method for wave-body interactions". *Journal of Computational Physics,* ***228***(17), pp. 6590–6616.

[3] Yang, J., and Balaras, E., 2006. "An embedded-boundary formulation for large-eddy simulation of turbulent flows interacting with moving boundaries". *Journal of Computational Physics,* ***215***(1), pp. 12–40.

[4] Osher, S., and Sethian, J. A., 1988. "Fronts propagating with curvature-dependent speed: Algorithms based on Hamilton–Jacobi formulations". *Journal of Computational Physics,* ***79***(1), pp. 12–49.

[5] Liu, X.-D., Fedkiw, R. P., and Kang, M., 2000. "A boundary condition capturing method for Poisson's equation on irregular domains". *Journal of Computational Physics,* ***160***(1), pp. 151–178.

[6] Yang, J., Preidikman, S., and Balaras, E., 2008. "A strongly coupled, embedded-boundary method for fluid-structure interactions of elastically mounted rigid bodies". *Journal of Fluids and Structures,* ***24***(2), pp. 167–182.

[7] de Tullio, M. D., Cristallo, A., Balaras, E., and Verzicco, R., 2009. "Direct numerical simulation of the pulsatile flow through an aortic bileaflet mechanical heart valve". *Journal of Fluid Mechanics,* ***622***, pp. 259–290.

[8] Kim, D., and Choi, H., 2006. "Immersed boundary method for flow around an arbitrarily moving body". *Journal of Computational Physics,* ***212***(2), pp. 662–680.

[9] Beddhu, M., Taylor, L. K., and Whitfield, D. L., 1996. "Strong conservative form of the incompressible Navier-Stokes equations in a rotating frame with a solution procedure". *Journal of Computational Physics,* ***128***(2), pp. 427–437.

[10] Sussman, M., Smereka, P., and Osher, S., 1994. "A level set approach for computing solutions to incompressible two-phase flow". *Journal of Computational Physics,* ***114***(1), pp. 146–159.

[11] Leonard, B. P., 1979. "A stable and accurate convective modelling procedure based on quadratic upstream interpolation". *Computer Methods in Applied Mechanics and Engineering,* ***19***(1), pp. 59–98.

[12] Jiang, G.-S., and Shu, C.-W., 1996. "Efficient implementation of weighted ENO schemes". *Journal of Computational Physics,* ***126***(1), pp. 202–228.

[13] Falgout, R., Jones, J., and Yang, U., 2006. "The design and implementation of hypre, a library of parallel high performance preconditioners". In *Numerical Solution of Partial Differential Equations on Parallel Computers*, A. Bruaset and A. Tveito, eds., Vol. 51. Springer-Verlag, pp. 267–294. UCRL-JRNL-205459.

[14] Peng, D., Merriman, B., Osher, S., Zhao, H., and Kang, M., 1999. "A PDE-based fast local level set method". *Journal of Computational Physics,* ***155***(2), pp. 410–438.

[15] Jiang, G.-S., and Peng, D., 2000. "Weighted ENO schemes for Hamilton–Jacobi equations". *SIAM Journal on Scientific Computing,* ***21***(6), pp. 2126–2143.

[16] Shu, C.-W., and Osher, S., 1988. "Efficient implementation of essentially non-oscillatory shock-capturing schemes". *Journal of Computational Physics,* ***77***(2), pp. 439–471.

[17] Dütsch, H., Durst, F., Becker, S., and Lienhart, H., 1998. "Low-Reynolds-number flow around an oscillating circular cylinder at low Keulegan–Carpenter numbers". *Journal of Fluid Mechanics,* ***360***, pp. 249–271.

[18] Greenhow, M., and Lin, W., 1983. Nonlinear free-surface effects: experiments and theory. Technical Report 83-19, Department of Ocean Engineering, MIT, Cambridge, MA.

[19] Fekken, G., 2004. "Numerical simulation of free-surface flow with moving rigid bodies". PhD Thesis, University of GroningenU, The Netherlands.

[20] Herrmann, M., 2008. "A balanced force refined level set grid method for two-phase flows on unstructured flow solver grids". *Journal of Computational Physics,* ***227***(4), pp. 2674 – 2706.